BNL-228878-2025-JAAM

Nucleation and growth of polar clusters with in-phase tilts into a long-range ferroelectric matrix in a sodium niobate based complex relaxor

H. Kumar, S. Ghose

To be published in "Physical Review B"

June 2025

Photon Sciences

Brookhaven National Laboratory

U.S. Department of Energy

USDOE Office of Science (SC), Basic Energy Sciences (BES). Scientific User Facilities (SUF)

DISCLAIMER

Nucleation and growth of antiferrodistortive Polar nano regions into a long-range ferroelectric matrix in a Sodium Niobate-based complex relaxor

Harsh Kumar,[1] Sanjit Ghose,[2] Rudolph Erasmus,[3] and Saurabh Tripathi[1,*]

[1]*Department of Physics, Indian Institute of Technology (BHU), Varanasi, 221005, India*
[2]*National Synchrotron Light Source II, Brookhaven National Laboratory, Upton, New York 11973, USA*
[3]*School of Physics and Microscopy and Microanalysis Unit, University of the Witwatersrand, WITS, Private Bag 3, Johannesburg 2050, South Africa*

In this study, we have investigated the temperature dependence of atomic ordering at multiple length scales in a lead-free sodium niobate-based relaxor, i.e., 0.75$NaNbO_3$- 0.25$Ba_{0.9}Ca_{0.1}TiO_3$ (NN-25BCT) via Synchrotron X-ray diffraction, Raman spectroscopic, and Pair distribution function analysis. High-resolution Synchrotron X-ray powder diffraction(SXRD) measurements reveal a ferroelectric phase transition in a relaxor ferroelectric NN-25BCT below the Vogel-Fulcher freezing temperature($T_{vf} \approx 270$ K). **In addition, SXRD analysis demonstrates the competition between in-phase octahedral tilting and ferroelectricity using mode crystallography.** On the other hand, Raman spectroscopic analysis provides evidence of polar ordering for T> T_{vf}(with tetragonal symmetry) persisting up to the Burns temperature(T_B). Furthermore, Pair distribution function (PDF) analysis reveals the presence of a polar antiferrodistortive tetragonal phase with P4bm space group at short ranges throughout the studied temperatures (i.e., 110$\leq$ T$\leq$ 500 K), irrespective of non-polar long-range ordering above T_{vf}. Therefore, our measurements provide a direct evidence for the presence of polar ordering at short ranges and their gradual transformation into long-range polar ordering using an integrated multiscale structural analysis. As a result of a transition from relaxor to a ferroelectric phase in the vicinity of room temperature, NN-25BCT can be exploited for applications in pyroelectric detectors, electrocaloric devices, and multi-layered ceramic capacitors.

Relaxor Ferroelectrics(RFs) have consistently drawn attention of the scientific community owing to thermal stability and are suitability for various applications, *viz.,* multilayered ceramic capacitors, sensors, high-precision actuators applications etc. [1–5]. The origin of relaxor behaviour has been attributed to nanoscale heterogeneity formally known as Polar nano regions(PNRs) [4, 6]. These Polar nano regions (PNRs) appear below Burn's Temperature(T_B). Immediately below T_B, there exists a short-lived correlation among PNRs, which results in a zero time averaged polarization. Nucleation of PNRs starts from Burn's temperature, and their number and size grow on lowering temperatures. Polar nano-regions are dynamic at high temperatures, and their dynamics slows down on decreasing temperature, eventually forming a glass-like structure below Vogel-Fulcher freezing temperature (T_{vf}) [6]. Unlike conventional ferroelectrics, most of the relaxors do not exhibit a long-range ferroelectric ordering below T_{vf} [7]. However, for some relaxors, a long-range ferroelectric ordering can be stabilized at low temperatures(below T_{vf}) on the application of external electric field [8]. Interestingly, there are a number of reports on relaxors showing transformation into a long-range ferroelectric state below T_{vf} without the application of electric field [9–13]. In light of the above discussion, relaxors can be divided into two categories based on the behaviour demonstrated by them below T_{vf}. The first category includes relaxors exhibiting a long-range ferroelectric order below T_{vf} (e.g. $PbMg_{1/3}Nb_{2/3}O_3$-x$PbTiO_3$ (PMN-PT))[12] while second category does not experiences a phase transition even at the cryogenic temperatures and demonstrates an average cubic structure (e.g. $PbMg_{1/3}Nb_{2/3}O_3$ (PMN)) [14, 15]. Various models have been proposed to explain the long-range ferroelectric phase transition at low temperatures in relaxors [9, 10].

For decades, lead-based relaxor materials have been in vogue, but concerns over the toxic effects of lead on human health led researchers to explore lead-free alternatives that can provide similar properties [2]. In our earlier work, we reported a solid solution of $NaNbO_3$(NN) and $Ba_{0.9}Ca_{0.1}TiO_3$ (BCT), where 0.75 $NaNbO_3$- 0.25($Ba_{0.9}Ca_{0.1}$)TiO_3 (NN-25BCT) demonstrates relaxor behaviour [16]. In this letter, we report the temperature evolution of short, medium and long-range crystal structure of NN-25BCT in a wide temperature range (110 K $\leq$ T $\leq$ 500 K). Dielectric analysis demonstrates nucleation and growth of polar nano-regions (PNRs) below Burns temperature (T$\leq$ T_B). Synchrotron X-ray diffraction(SXRD) data clearly reveals relaxor to ferroelectric phase transition in NN-25BCT at low temperature (T $\leq$ T_{vf}). Distortion mode analysis of the low-temperature ferroelectric phase(SG: P4bm) provides an experimental evidence of competitive interactions between ferroelectricity and in-phase octahedral rotations. Raman spectroscopy and Pair Distribution function analysis, in conjunction with SXRD analysis, suggest the presence of local polar order for T > T_{vf} in the long-range paraelectric matrix.

For a detailed synthesis and experimental procedure, see the supplementary file. In our previous paper, we examined composition-dependent phase transitions of (1-x) $NaNbO_3$-x $Ba_{0.9}Ca_{0.1}TiO_3$ (NN-xBCT) for $0.00 \leq x \leq 1.00$. We observed a relaxor ferroelectric-like behaviour for x=0.25 characterised by a high diffusion coefficient (γ =1.94) [16]. Fig. 1(a) illustrates temperature-dependent real and imaginary parts of dielectric permittivity at various frequencies(1KHz-1MHz) in the wide temperature range (100 $\leq$ T $\leq$ 550 K). The real part of dielectric permittivity exhibits a diffuse nature around the maximum ($T_m \approx 285$ K) and demonstrates a typ-

* stripathi.phy@itbhu.ac.in

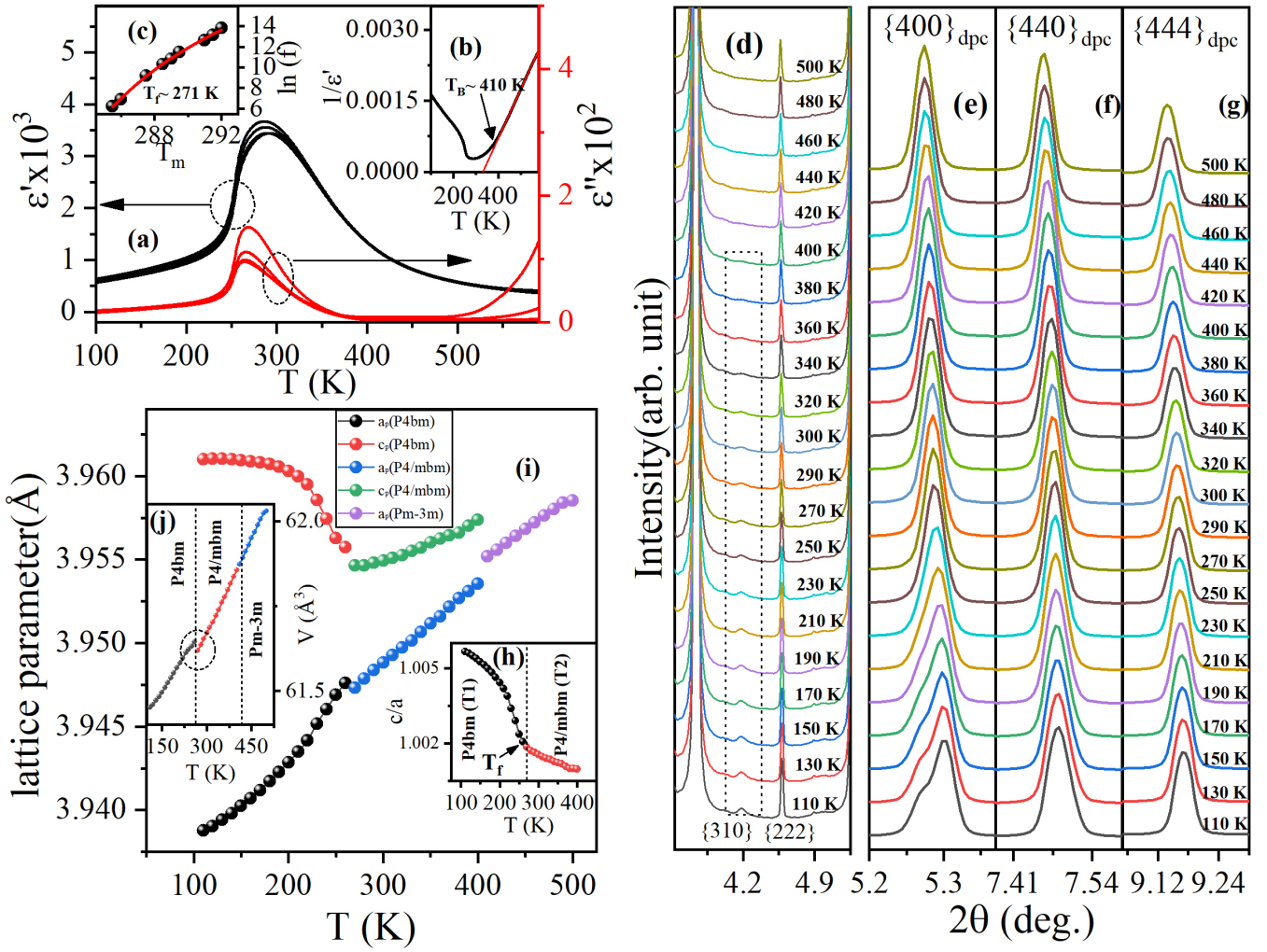

FIG. 1. (a) Temperature-dependent evolution of real and imaginary part of dielectric permittivity. (b) The inverse of dielectric permittivity as a function of temperature marking the Burn's Temperature(c)Vogel-Flucher fitting of the temperatures corresponding to the dielectric to estimate the freezing temperature. Temperature-dependent evolution of (d) superlattice reflections (e-g) main perovskite reflections. (h) variation of tetragonality of the unit cell. Evolution of (i) lattice parameters (j)volume of the elementary cell.

ical relaxor behaviour. The relaxor behaviour in the present system can be attributed to the presence of multiple cations with different oxidation states/sizes occupying the same crystallographic site, resulting in local strain and local fields simultaneously. Fig 1(b) shows the inverse of dielectric permittivity as a function of temperature at 10 kHz. For NN-25BCT, the dielectric permittivity deviates from the Curie-Weiss law above T_m but exhibits linear behaviour above T ≈ 410 K. The temperature at which this deviation starts is referred to as the Burns temperature(T_B). It is also known that the nucleation and growth of the polar nano regions(PNRs) start at Burns temperature. At high temperatures(but below T_B), these PNRs are mobile, and their dynamics slow down on cooling. The PNRs freeze in a glass-like state below a temperature(T_{vf}), which can be determined using the Vogel-Flucher(V-F) relation.

$$f = f_0 \exp\left[-\frac{E_a}{k(T_{max} - T_{vf})}\right] \quad (1)$$

where T_{vf} is the static freezing temperature, E_a is the activation energy, f_o is an attempt frequency, and T_{max} is the temperature of the dielectric permittivity maximum [17, 18]. Fig. 1(c) shows Vogel- Fulcher fitting of the real part of the permittivity of NN-25BCT. in the frequency range of 500 Hz to 1 MHz. The data was well-fitted by Vogel-Fulcher equation with pre-exponential factor f_o=7.68 x 10^{12} Hz, activation energy E_a= 0.028 eV and Vogel-Fulcher freezing temperature T_{vf} ≈ 271 K, respectively. These values closely align with those reported in similar studies [2, 19]. It has been reported earlier that relaxors with activation energy close to the present value transform into a long-range ferroelectric phase at low temperatures [9]. Therefore, we aim to explore relaxor-ferroelectric phase transition below freezing tempera-

ture T_{vf}(if any).

To explore temperature-dependent structural phase transitions of NN-25BCT, we have performed Synchrotron X-ray diffraction measurements. The indexing of the diffraction pattern has been done with respect to a doubled perovskite cell(dpc). Fig.1(e)-(g) depicts main perovskite reflections *viz.*, $\{400\}_{dpc}$, $\{440\}_{dpc}$, and $\{444\}_{dpc}$ for a wide temperature range ($110 \leq T \leq 500$ K). Fig. 1(d) demonstrates the appearance of the superlattice reflection(s) on decreasing temperature. At 500 K, all the reflections are singlet in nature: a typical feature of high-temperature phase in relaxors having a cubic structure with $Pm\bar{3}m$ space group [10, 20]. At low temperatures, a weak shoulder appears near $\{400\}_{dpc}$ at a lower 2θ and $\{440\}_{dpc}$ becomes asymmetric. Moreover, we see the appearance of a weak superlattice reflection near $\{222\}_{dpc}$ reflection for T≤400. This weak reflection was indexed as $\{310\}$ with respect to doubled perovskite cell and is associated with in-phase octahedral rotation [21]. The superlattice reflection remains stable down to the lowest studied temperature, i.e., 110 K. The main perovskite reflections, *viz.*, $\{hoo\}_{dpc}$ and $\{hho\}_{dpc}$ spit, whereas $\{hhh\}_{dpc}$ reflections remain singlet, suggesting a tetragonal symmetry. Such splitting of main perovskite reflections has been observed for pure $NaNbO_3$ at high temperatures[SG: P4/mbm(paraelectric); tilt system: $a_0^0a_0^0c_0^+$] and $BaTiO_3$ at ambient conditions[SG: P4mm(ferroelectric)] [22]. However, the presence of superlattice reflections along with splitting in the main perovskite reflections of NN-25BCT discards Barium Titanate-like tetragonal phase(SG: P4mm), which results only due to octahedral distortion. Following the literature on similar systems, a plausible ferroelectric tetragonal phase with in-phase octahedral rotations is P4bm space group(tilt system: $a_0^0a_0^0c_+^+$, cell size: $\sqrt{2}a_p \times \sqrt{2}a_p \times c_p$) which can be visualized as a 'polar version' of the tilt orientated tetragonal phase observed in the paraelectric region of $NaNbO_3$ (with P4/mbm space group) [21–23]. The presence of a superlattice reflection (due to an in-phase octahedral tilt) and splitting of the main perovskite reflections suggest a paraelectric tetragonal phase with a P4/mbm(T1) space group at ambient conditions. Nonetheless, a ferroelectric tetragonal model (SG: P4bm(T2)) is plausible below the V-F freezing temperature, i.e., $T_{vf} \approx 270$ K. To confirm the evolution of the crystallographic phases as a function of temperature, Rietveld refinements of the diffraction patterns have been carried out using the FULLPROF package [24]. We have used the following models to fix the diffraction pattern **(i)**$Pm\bar{3}m$(PE): for 500≤ T≤ 410 K **(ii)** P4/mbm (PE): for 400≤ T≤ 270 K **(iii)** P4bm (FE): for 260≤ T≤ 110 K. The choice of these models has been made on the basis of splitting in main perovskite reflections and the appearance of superlattice reflections on decreasing temperature. The transition from a centrosymmetric tetragonal phase with P4/mbm space group (paraelectric) to a non-centrosymmetric tetragonal phase with P4bm space group (ferroelectric) is evident from a discontinuity in the unit cell volume and a non-analytical behaviour in tetragonality around T≈270 K which also coincides with the V-F freezing temperature T_{vf}≈270 K (see Fig. 1(h) & 1(j)). Similar characteristics of the phase transition are also observed for (PMN-PT, PZN) where relaxors undergo a long-range ferroelectric phase transition below Vogel-Fulcher freezing temperature(T_{vf})[9–13]. Fig. S1 in the supplementary file depicts the fitted diffraction patterns of NN-25BCT for some representative temperatures. Table S1 presents the lattice parameters, atomic coordinates and thermal parameters obtained after refinements of the diffraction patterns collected at 110 K and 300 K, using P4bm and P4/mbm space groups, respectively(see supplementary file). Fig. 1(i) shows the evolution of reduced lattice parameters as a function of temperature. Henceforth, Rietveld refined fits, along with reasonable agreement factors, suggest a long-range ferroelectric order below V-F freezing temperature(T_{vf})in the present system exhibiting relaxor-like characteristics. Unlike lead-based relaxor systems, which display an average cubic structure with rhombohedral clusters at short ranges that transforms into a long-range rhombohedral phase below the freezing temperature(T_{vf}), NN-25BCT exhibits an average centrosymmetric tetragonal structure (SG: P4/mbm) at room temperature. This phase transforms into a non-centrosymmetric tetragonal ferroelectric phase(SG: P4bm) upon cooling.

The structure of an ideal perovskite is cubic with $Pm\bar{3}m$ space group [25]. However, most of the perovskites are distorted at ambient conditions, exhibiting fascinating properties.

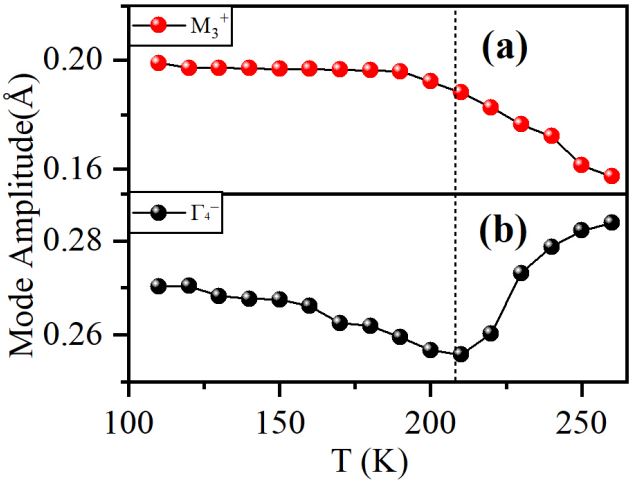

FIG. 2. Temperature-dependent evolution of (a) M_3^+ and (b) Γ_4^- for the long-range ferroelectric phase P4bm.

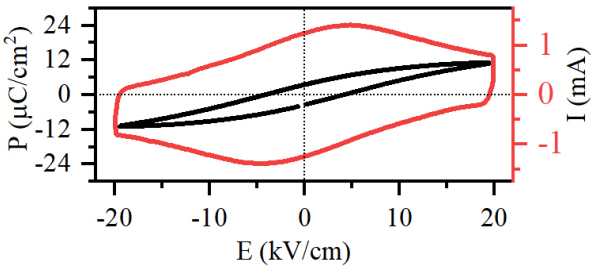

FIG. 3. Room temperature P-E and I-E curve of NN-25BCT measured at a maximum electric field of 20 kV/cm. The slim hysteresis loop is characteristic of a relaxor-like behaviour.

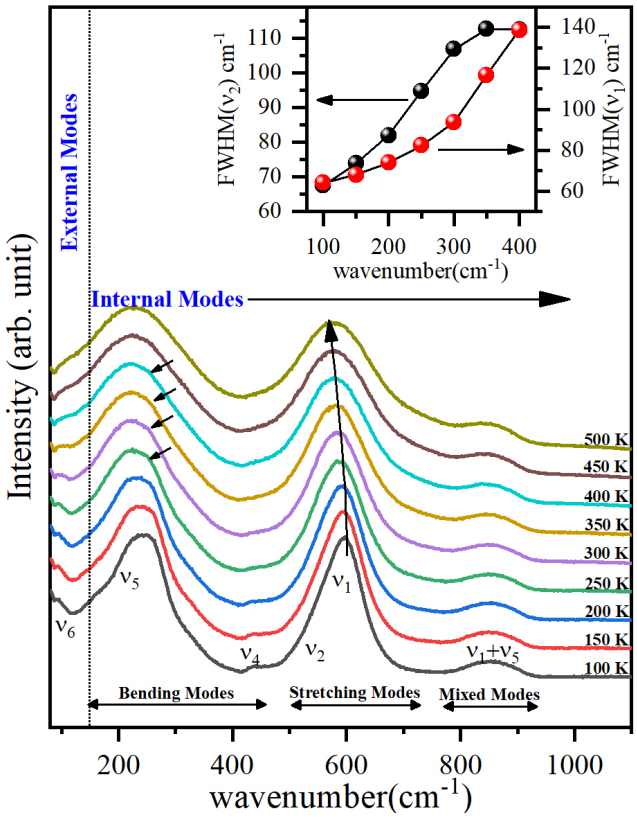

FIG. 4. Variable temperature Raman spectra of NN-25BCT at different temperatures in the range of 100-500 K. The Raman spectra have been taken during the heating cycle using the protocol described in the experimental section. The inset shows the FWHM for ν_1 and ν_2 Raman modes.

There exist three different types of distortions: (i) distortion of BO_6 octahedra, (ii) cationic displacements, and (iii) tilting of BO_6 octahedra with respect to each other [26, 27]. Identical displacements of B-site cations are responsible for ferroelectricity, and such distortions are linked with the Γ(k=0,0,0) point of the cubic billion zone. On the other hand, in-phase and out-of-phase octahedral tilting results in cell multiplication and are linked with M(k=1/2,1/2,0) and R(k=1/2,1/2,1/2) points of cubic Brillouin zone [26, 27]. The distortions present in the low-symmetry structures correspond to a mode(s) that are soft in the high-symmetry cubic structure [28, 29]. Further, these distortion modes are associated with the irreducible representations of the parent space group [28, 29]. Symmetry mode analysis has been performed to quantify the contribution of different modes in the low-symmetry distorted structure. In the present work, the low-temperature phase of NN-25BCT is ferroelectric, having a tetragonal symmetry with P4bm space group(tilt system: $a^0_0a^0_0c^+_+$). For quantifying the structural distortions, we used *AMPLIMODES* program available at the Bilbao Crystallographic server [28, 29]. As input for *AMPLIMODES*, we have used the high-symmetry cubic phase (SG: Pm$\bar{3}$m & a_0= 3.95854 Å) as a reference(parent) structure and the low-symmetry tetragonal(SG: P4bm) phase as a distorted structure. To describe the atomic positions of the undistorted cubic phase, we have used a Wyckoff sequence in which A, B, and O atoms occupy 1b(1/2,1/2,1/2), 1a(0,0,0), and 3d(1/2,0,0) sites, respectively. The transition from cubic phase to the tetragonal phase occurs through the splitting of the Wyckoff sites(see Table I). As indicated in Table I, the two modes, Γ_4^- and M_3^+, are responsible for the symmetry-breaking transition from Pm$\bar{3}$m → P4bm. These irreducible representations(irrep) *viz.*, M_3^+ and Γ_4^- are linked with the zone boundary and the zone centre of the cubic Brillouin zone, leading to in-phase rotations of adjacent octahedra and ferroelectric displacements in the unit cell, respectively. Therefore, we can quantify in-phase octahedral rotations and ferroelectric displacements by calculating the amplitudes of M_3^+ and Γ_4^- modes using *AMPLIMODES*. **Now, the effect of octahedral rotations on ferroelectricity in the perovskite-based systems has been a matter of discussion for several decades [30–33].** Generally, ferroelectricity(polar displacements) in perovskite-based systems increase with decrease in temperatures, and hence, the amplitude of the Γ_4^- phonon mode would increase with decreasing temperatures [34]. Fig. 2 illustrates the temperature-dependent evolution of the amplitude of Γ_4^- and M_3^+ modes. From 260 K to 220 K, the amplitude of M_3^+ mode increases and reaches its saturation value below 200 K. On the other hand, the amplitude of the Γ_4^- mode initially decreases up to 200 K, after which it increases with decreasing temperature. It is important to note that the amplitude of the Γ_4^- mode starts showing its obvious effect (i.e., increase in amplitude with the decrease in temperature) once the amplitude of M_3^+ mode reaches saturation. It is widely reported in the literature that octahedral tilts have detrimental effects on ferroelectricity, as they tend to suppress it[32, 33, 35–37], which can be observed as a reduction in the amplitude of the Γ_4^- mode. Thus, our experimental science results provide evidence of the competitive nature of octahedral rotations with ferroelectric displacements in perovskites using the mode crystallographic approach.

TABLE I. Wyckoff site splitting in high- and low-symmetry structures with corresponding symmetry breaking modes. Here, A and B represent the atoms positioned at the A and B sites of the perovskite structure.

Wyckoff site splitting		
SG: Pm$\bar{3}$m	**Symmetry breaking modes**	**SG: P4bm**
A 1a	Γ_4^-	A 2b
B 1b	Γ_4^-	B 2a
O 3d	Γ_4^-, M_3^+	O1 2a, O2 4c

Fig. 3 shows the P-E and I-E curves at room temperature at a maximum field of 20 kV/cm. It is important to note that the slim hysteresis (P-E) loop and the switching peaks in the I-E curve suggest ferroelectric characteristics contrary to the long-range centrosymmetric structure with a tetragonal symmetry (SG: P4/mbm) at room temperature(i.e., 300 K). This ferroelectric response likely stems from short-range ordering observed in Polar nano regions typical to relaxors. In order to explore short-range ordering and their symmetry, temperature-dependent Raman spectroscopy (RS) has

been employed [16, 38–40]. Fig. 4 shows the temperature-dependent evolution of Raman spectra collected in the temperature range 100 ≤ T ≤ 500 K. All the Raman spectra were corrected for the Bose-Einstein population factor [41]. The Raman spectra can be decomposed into two distinct types of modes: (i) Motion of A-site cation with respect to BO_6 octahedra(external modes) and (ii) Isolated vibration of BO_6 octahedra which involve bending and stretching modes(internal modes) [42]. At the lowest temperature(i.e., T=100 K), there are three prominent peaks are present around ≈250 cm^{-1} (ν_5), ≈ 600 cm^{-1} (ν_1), and ≈ 850 cm^{-1} (ν_1+ν_5). Here ν_5 and ν_4 are bands corresponding to bending motion of BO_6 octahedra while ν_1 and ν_2 corresponds to symmetric and asymmetric stretching associated with O-Nb-O bonds. Significant Raman scattering has been detected at 500 K, where the long-range structure is $Pm\bar{3}m$, with all atoms positioned at sites possessing a centre of inversion. Consequently, first-order Raman scattering should be forbidden under these conditions. Such Raman Scattering is often attributed to cationic disorder or second-order effects [40, 42]. Further, for T≤ 400 K, we can see the evolution of a shoulder around the broad peak at ≈ 250 cm^{-1}. It is important to mention that for NN-25BCT, a long-range polar phase exists only below the V-F freezing temperature T_{Vf}(≈ 270 K). Therefore, these findings offer strong evidence for the presence of ferroelectric ordering at short ranges(PNRs) for T≤ 400 K. Similar Raman spectra have also been reported earlier in related systems, where the ferroelectric ordering with tetragonal symmetry has been observed at smaller length scales(short-range order) [21, 43]. All the Raman spectra were fitted using a suitable number of Lorentz peaks (see Fig. S2 in the supplementary file). The ν_1 and ν_5 modes exhibited a clear shift to lower wavenumbers as temperature increases, indicating a gradual softening of the B-O vibrations. This softening is attributed to the weakening of the bond between the B-site cations and oxygen due to increased B-O bond lengths at high temperatures. The softening of phonon modes and a noticeable increase in the full width at half maximum (FWHM) for the ν_1 and ν_2 modes reflect an increase in structural disorder and reduction in unit cell polarity(see inset of Fig. 3).

Generally, it has been observed that the symmetry at short-ranges(PNRs) in relaxors is lower than the symmetry at long-range [22, 44–48]. Pair distribution function analysis(PDF) is widely used for quantitative analysis of short-range structural distortions [49, 50]. Fig. S3 shows the temperature-dependent PDF profiles of NN-25BCT in a wide temperature range, i.e., 110-500 K(see supplementary file). To determine a plausible short-range structural model, we simulated Pair Distribution Function (PDF) profiles for several closely related phases (see Fig. 5). In many systems, it has been reported that the long-range symmetry at low temperatures matches with the symmetry of the short ranges (PNRs) at high-temperature non-polar phase [9, 10, 14, 20]. For clarity, we simulated three probable tetragonal phases: (i) P4bm: tilt-oriented(antiferrodistortive) ferroelectric; (ii) P4mm: the tilt-free ferroelectric; and (iii) P4/mbm: tilt-oriented(antiferrodistortive) paraelectric phase. In the simulations, the volume of the unit cell was kept the same for

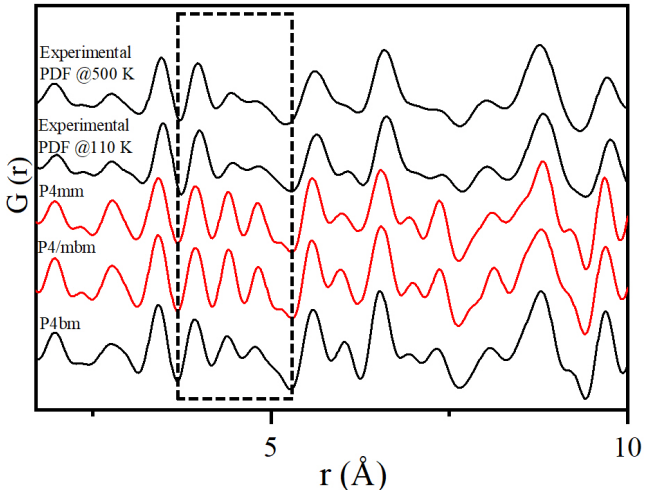

FIG. 5. Comparison of simulated PDF profiles with the experimental PDFs at 110 K and 500 K.

all three models. Fig. 5 compares the experimental PDF with these potential models. While all models exhibit similar characteristics, the P4bm model aligns more closely with the experimental data, as indicated by the peak profiles in the highlighted region. Consequently, we conclude that the short-range symmetry is the same as the long-range symmetry at low temperatures(i.e., tetragonal with P4bm space group). As the temperature increases, no sharp transitions are observed, with peak broadening attributed to increased thermal disorder at higher temperatures. Thus, we can conclude that no structural phase transition occur at short ranges within the studied temperature range(110 K ≤ T ≤ 500 K).

In summary, the dielectric analysis of NN-25BCT reveals relaxor-like behaviour with a freezing temperature T_{vf} ≈ 270 K. Further, SXRD confirms a long-range relaxor(SG: P4/mbm) to ferroelectric (SG: P4bm) phase transition at low temperatures (T<T_{vf}). **Our experimental work clearly reveals that in-phase octahedral tilting suppresses ferroelectricity in the perovskite-based systems**. Temperature-dependent Raman spectra reveal local polar distortions for temperatures above T_{vf} contrary to the long-range centrosymmetric structure obtained from SXRD. Further, PDF analysis provides evidence of local distortions with ferroelectric tetragonal ordering(SG: P4bm) stable throughout the studied temperature range, i.e., 110 K ≤ T ≤ 500 K. Therefore, it is reasonable to believe that the relaxor to ferroelectric phase transition originates from the nucleation and growth of short-range ordered polar tetragonal phase (PNRs with P4bm symmetry) present in a long-range centrosymmetric matrix (with P4/mbm space group). Thus, relaxor ferroelectric NN-25BCT can be a potential candidate for applications in pyroelectric detectors, electrocaloric devices, Multi-layered ceramic capacitors(MLCCs), etc.

[1] S.-E. Park and T. R. Shrout, Ultrahigh strain and piezoelectric behavior in relaxor based ferroelectric single crystals, Journal of applied physics **82**, 1804 (1997).

[2] V. V. Shvartsman and D. C. Lupascu, Lead-free relaxor ferroelectrics, Journal of the American Ceramic Society **95**, 1 (2012).

[3] C. W. Ahn, C.-H. Hong, B.-Y. Choi, H.-P. Kim, H.-S. Han, Y. Hwang, W. Jo, K. Wang, J.-F. Li, J.-S. Lee, *et al.*, A brief review on relaxor ferroelectrics and selected issues in lead-free relaxors, Journal of the Korean Physical Society **68**, 1481 (2016).

[4] A. Bokov and Z.-G. Ye, Recent progress in relaxor ferroelectrics with perovskite structure, Journal of materials science **41**, 31 (2006).

[5] A. Tripathi, A. Pandey, J. A. Alonso, R. Erasmus, M. T. Fernandez-Diaz, and S. Tripathi, Origin of zero thermal expansion in an average cubic structure in Pb-free relaxor ferroelectrics, Applied Physics Letters **125** (2024).

[6] S. Kojima, R. Ohta, T. Ariizumi, and J. Zushi, Dynamic polar nanoregions and broken local symmetry in relaxor ferroelectrics probed by inelastic light scattering, in *Journal of Physics: Conference Series*, Vol. 428 (IOP Publishing, 2013) p. 012027.

[7] Y.-H. Bing, A. Bokov, and Z.-G. Ye, Diffuse and sharp ferroelectric phase transitions in relaxors, Current Applied Physics **11**, S14 (2011).

[8] J. Zhao, A. Glazounov, Q. Zhang, and B. Toby, Neutron diffraction study of electrostrictive coefficients of prototype cubic phase of relaxor ferroelectric $PbMg_{1/3}Nb_{2/3}O_3$, Applied physics letters **72**, 1048 (1998).

[9] F. Chu, I. Reaney, and N. Setter, Investigation of relaxors that transform spontaneously into ferroelectrics, Ferroelectrics **151**, 343 (1994).

[10] X. Dai, Z. Xu, and D. Viehland, The spontaneous relaxor to normal ferroelectric transformation in La-modified lead zirconate titanate, Philosophical Magazine B **70**, 33 (1994).

[11] V. R. Mastelaro, Y. P. Mascarenhas, P. Neves, M. Mir, A. C. Doriguetto, A. Michalowicz, J. Moscovici, M. Lente, and J. A. Eiras, Spontaneous long and short-range ferroelectric ordering in $Pb_{0.55}La_{0.3}TiO_3$ ceramics, Journal of Applied Physics **107** (2010).

[12] B. Dkhil, J. Kiat, G. Calvarin, G. Baldinozzi, S. Vakhrushev, and E. Suard, Local and long range polar order in the relaxor-ferroelectric compounds $PbMg_{1/3}Nb_{2/3}O_3$ and $PbMg_{0.3}Nb_{0.6}Ti_{0.1}O_3$, Physical Review B **65**, 024104 (2001).

[13] X. Dai and D. Viehland, Tetragonal-structured plzt relaxor ferroelectrics, Ferroelectrics **158**, 375 (1994).

[14] H. Arndt, F. Sauerbier, G. Schmidt, and L. Shebanov, Field-induced phase transition in $Pb(Mg_{1/3}Nb_{2/3})O_3$ single crystals, Ferroelectrics **79**, 145 (1988).

[15] X. Zhao, W. Qu, X. Tan, A. Bokov, and Z.-G. Ye, Electric field-induced phase transitions in (111)-,(110)-, and (100)-oriented $Pb(Mg_{1/3}Nb_{2/3})O_3$ single crystals, Physical Review B—Condensed Matter and Materials Physics **75**, 104106 (2007).

[16] H. Kumar and S. Tripathi, Similarities and differences in the ordering at short and long ranges in a $NaNbO_3$ based Pb-free smart system: a key to functional properties, Journal of Physics D: Applied Physics **57**, 335502 (2024).

[17] D. Viehland, S. Jang, L. E. Cross, and M. Wuttig, Freezing of the polarization fluctuations in lead magnesium niobate relaxors, Journal of Applied Physics **68**, 2916 (1990).

[18] X. Long and Z.-G. Ye, Relaxor behavior in the solid solution between dielectric $Ba(Mg_{1/3}Nb_{2/3})O_3$ and ferroelectric $PbTiO_3$, Applied physics letters **90** (2007).

[19] V. Shvartsman, J. Zhai, and W. Kleemann, The dielectric relaxation in solid solutions $BaTi_{1-x}Zr_xO_3$, Ferroelectrics **379**, 77 (2009).

[20] F. Chu, I. Reaney, and N. Setter, Spontaneous (zero-field) relaxor to ferroelectric-phase transition in disordered $Pb(Sc_{1/2}Nb_{1/2})O_3$, Journal of applied physics **77**, 1671 (1995).

[21] L. Wang, H. Qi, B. Gao, Y. Liu, H. Liu, and J. Chen, Large piezoelectricity in $NaNbO_3$-based lead-free ceramics via tuning oxygen octahedral tilt, Materials Horizons **9**, 1002 (2022).

[22] L. Jiang, D. Mitchell, W. Dmowski, and T. Egami, Local structure of $NaNbO_3$: A neutron scattering study, Physical Review B—Condensed Matter and Materials Physics **88**, 014105 (2013).

[23] Z. Wang, Z. An, J. Zhuang, F. Li, W. Ren, Z.-G. Ye, and N. Zhang, Origin of polar nanoregions from displacive correlation in relaxor ferroelectric $Pb(Mg_{1/3}Nb_{2/3})O_3$–$PbTiO_3$, Journal of Materials Chemistry C **10**, 16731 (2022).

[24] J. Rodríguez-Carvajal, Recent advances in magnetic structure determination by neutron powder diffraction, Physica B: Condensed Matter **192**, 55 (1993).

[25] M. E. Lines and A. M. Glass, *Principles and applications of ferroelectrics and related materials* (Oxford university press, 2001).

[26] A. M. Glazer, The classification of tilted octahedra in perovskites, Acta Crystallographica Section B: Structural Crystallography and Crystal Chemistry **28**, 3384 (1972).

[27] A. Glazer, Simple ways of determining perovskite structures, Acta Crystallographica Section A: Crystal Physics, Diffraction, Theoretical and General Crystallography **31**, 756 (1975).

[28] D. Orobengoa, C. Capillas, M. I. Aroyo, and J. M. Perez-Mato, AMPLIMODES: symmetry-mode analysis on the Bilbao Crystallographic Server, Journal of Applied Crystallography **42**, 820 (2009).

[29] J. Perez-Mato, D. Orobengoa, and M. Aroyo, Mode crystallography of distorted structures, Acta Crystallographica Section A: Foundations of Crystallography **66**, 558 (2010).

[30] W. Zhong and D. Vanderbilt, Competing structural instabilities in cubic perovskites, Physical review letters **74**, 2587 (1995).

[31] N. Sai and D. Vanderbilt, First-principles study of ferroelectric and antiferrodistortive instabilities in tetragonal $SrTiO_3$, Physical Review B **62**, 13942 (2000).

[32] U. Aschauer and N. A. Spaldin, Competition and cooperation between antiferrodistortive and ferroelectric instabilities in the model perovskite $SrTiO_3$, Journal of Physics: Condensed Matter **26**, 122203 (2014).

[33] N. A. Benedek and C. J. Fennie, Why are there so few perovskite ferroelectrics?, The Journal of Physical Chemistry C **117**, 13339 (2013).

[34] H. Wieder, Electrical behavior of Barium Titanate single crystals at low temperatures, Physical Review **99**, 1161 (1955).

[35] C.-J. Eklund, C. Fennie, and K. Rabe, Strain-induced ferroelectricity in orthorhombic $CaTiO_3$ from first principles, Physical Review B—Condensed Matter and Materials Physics **79**, 220101 (2009).

[36] S. Bhattacharjee, E. Bousquet, and P. Ghosez, Engineering multiferroism in $CaMnO_3$, Physical review letters **102**, 117602 (2009).

[37] A. J. Hatt and N. A. Spaldin, Structural phases of strained $LaAlO_3$ driven by octahedral tilt instabilities, Physical Review B—Condensed Matter and Materials Physics **82**, 195402 (2010).

[38] S. Gupta, R. Katiyar, R. Guo, and A. Bhalla, Study of structural phase transitions in solid-solution (1-x)PZN-xPT relaxor ferroelectric using Raman scattering, Journal of Raman Spectroscopy **31**, 921 (2000).

[39] P. Dobal, R. Katiyar, and C.-S. Tu, Study of ordered nanoregions in $Pb(Zn_{1/3}Nb_{2/3})_{0.915}Ti_{0.085}O_3$ single crystal using Raman spectroscopy, Journal of Raman Spectroscopy **34**, 152 (2003).

[40] J. Kreisel and P. Bouvier, High-pressure Raman spectroscopy of nano-structured ABO_3 perovskites: a case study of relaxor ferroelectrics, Journal of Raman Spectroscopy **34**, 524 (2003).

[41] O. Svitelskiy, J. Toulouse, G. Yong, and Z.-G. Ye, Polarized Raman study of the phonon dynamics in $Pb(Mg_{1/3}Nb_{2/3})O_3$ crystal, Physical Review B **68**, 104107 (2003).

[42] P. Krishna, S. Mishra, A. Shinde, S. Kesari, and R. Rao, Raman spectroscopy of Lithium modified Sodium Niobate at elevated temperature, Ferroelectrics **510**, 34 (2017).

[43] R. Zuo, H. Qi, J. Fu, J.-F. Li, and L. Li, Multiscale identification of local tetragonal distortion in $NaNbO_3$-$BaTiO_3$ weak relaxor ferroelectrics by Raman, synchrotron x-ray diffraction, and absorption spectra, Applied Physics Letters **111** (2017).

[44] K. A. Schönau, L. A. Schmitt, M. Knapp, H. Fuess, R.-A. Eichel, H. Kungl, and M. J. Hoffmann, Nanodomain structure of $Pb[Zr_{1-x}\ Ti_x]O_3$ at its morphotropic phase boundary: Investigations from local to average structure, Physical Review B—Condensed Matter and Materials Physics **75**, 184117 (2007).

[45] I. Grinberg, V. R. Cooper, and A. M. Rappe, Relationship between local structure and phase transitions of a disordered solid solution, Nature **419**, 909 (2002).

[46] T. Egami, W. Dmowski, M. Akbas, and P. Davies, Local structure and polarization in Pb containing ferroelectric oxides, in *AIP Conference Proceedings*, Vol. 436 (American Institute of Physics, 1998) pp. 1–10.

[47] W. Dmowski, M. Akbas, P. Davies, and T. Egami, Local structure of Pb $(Sc_{1/2},Ta_{1/2})O_3$ and related compounds, Journal of Physics and Chemistry of Solids **61**, 229 (2000).

[48] T. Egami, Local structure of ferroelectric materials, Annu. Rev. Mater. Res. **37**, 297 (2007).

[49] S. J. Billinge, The atomic pair distribution function: past and present, Zeitschrift für Kristallographie-Crystalline Materials **219**, 117 (2004).

[50] S. J. Billinge and M. G. Kanatzidis, Beyond crystallography: the study of disorder, nanocrystallinity and crystallographically challenged materials with pair distribution functions, Chemical communications , 749 (2004).